Module 4: Interferometry

Lecture 19: Fringe analysis and image processing

## The Lecture Contains:

Image processing

- Fringe Thinning Algorithm
- Automatic Fringe Thinning Algorithm
- Curve Fitting Approach
- Paint Brush Drawing
- Comparison of Fringe Thinning Algorithms
- Closure

Previous Next

## Image Processing

The information generated by Mach-Zehnder interferometer is available in the form of interference fringes. The interferograms contains information about the temperature itself in two-dimensional fields. In three-dimensional problems, interferograms must be recorded at various projection angles and must scan the complete fluid domain. Temperature distribution can subsequently be determined by interpreting the interferometric images as path integrals and applying principles of three-dimensional reconstruction. Tomographic alogorithms are applicable in this context. Tomography falls in the class of inverse techniques and its performance is characterized by a definite dependence on noise levels in the prescribed data. Specifically, errors in data can be amplified during the reconstruction process. It is thus natural to examine the sensitivity of the reconstructed temperature field to uncertainties and errors that are intrinsic to image enhancement operations that required processing the interferograms. For both two- and three-dimensional measurements, the fringe patters thus have to be analyzed in detail.

One of the operations required most often is the extraction of the fringe skeleton from the dark and bright bands of the fringes. When the interferometer is operated in the infinite fringe setting, the fringes are a set of curves that are the locus of points having an identical path difference. This can be interpreted as follows: For rays having a certain path difference, the corresponding pixels in the interferometric image will have identical light intensity. One of the direct ways to locate a typical locus of points is to connect all minimum intensity pixels within a dark band or the maximum intensity pixels within a bright band. The minimum intensity will appear at a point of complete destructive interference and hence will have a zero intensity. Similarly, a maximum in intensity will appear at a point where interference is constructive.

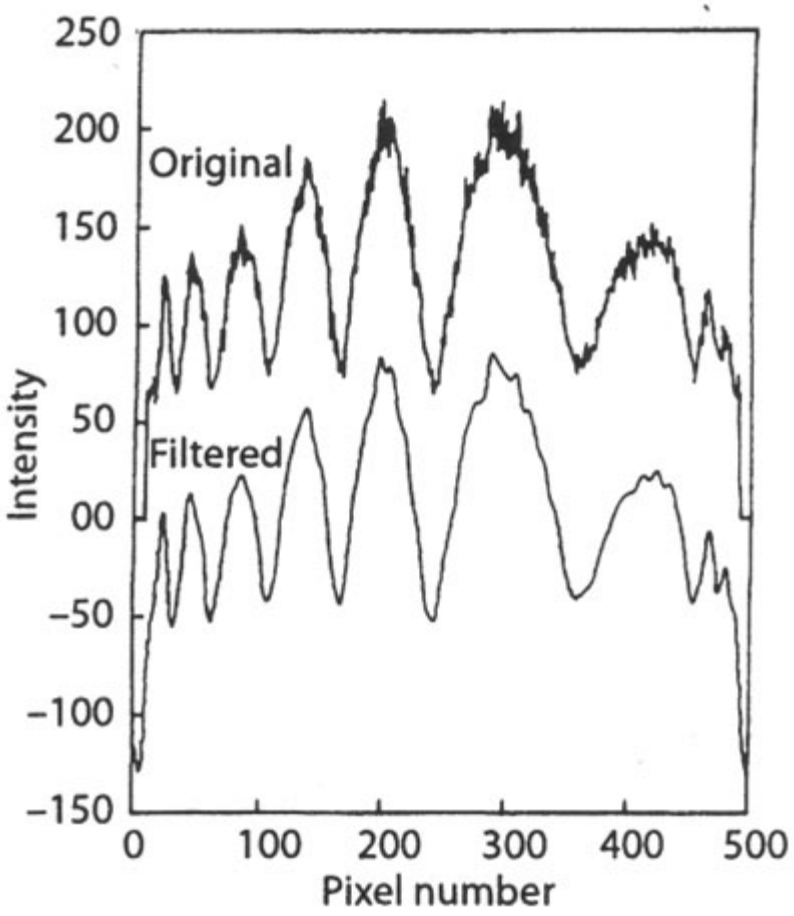


Figure 4.16: Original and filtered intensity distributions in an interferogram.

more...

Previous Next

## Fringe Thinning Algorithms

Three fringe thinning algorithms suitable for Interferograms recorded using the Mach-Zehnder interferometer are presented in this section. The first is an automatic technique for fringe thinning using the intensity minima within a dark band and does not require user intervention. This has been compared to two other methods of approximately locating the intensity minima. These are: (1) the midpoint search within a dark band, and (2) paintbrush drawing using a personal computer.

### Automatic Fringe Thinning Algorithm

The algorithm under discussion is similar to the one proposed by Funnell [86], but in view of certain differences in the direction of the minimum intensity. The direction is decided by using the intensity information over a template of pixels. The computer code developed in the present study can run using different sizes of templates and handle complex fringe shapes. The input required for the code are the starting points arbitrarily selected for each of the fringes.

The algorithm uses the following ideas. The direction of the tracings are defined as: (a) forward, and (b) backward, (Fig 4.17)

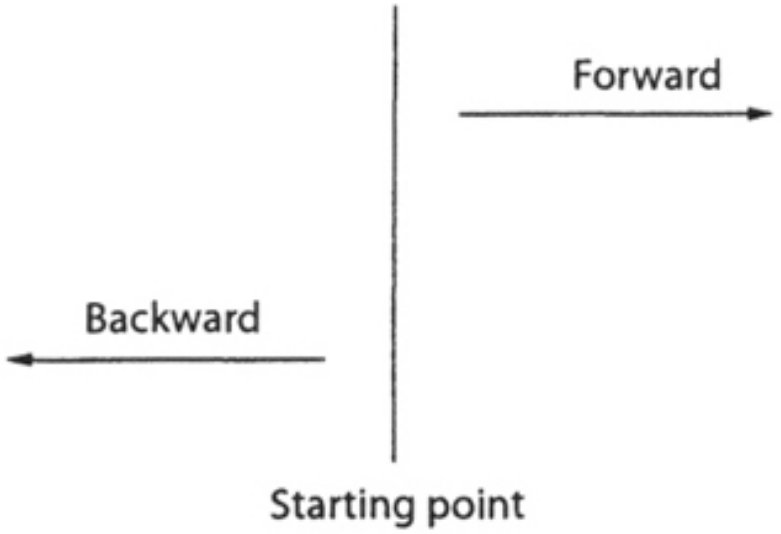


Figure 4.17: Two major directions for tracing of fringes

The turning of fringes by more than $\pm 90$ degrees results in a change of direction and is a special case. Such areas of the fringes where a turning occurs has to be predefined in the form of a rectangle covering the area. These cases are classified into four categories depending on the angle of turning: (a) while in forward direction turning backward up, (b) while in forward direction turning backward down, (c) while in backward direction turning forward up, (d) while in backward direction turning forward down (fig.4.18).

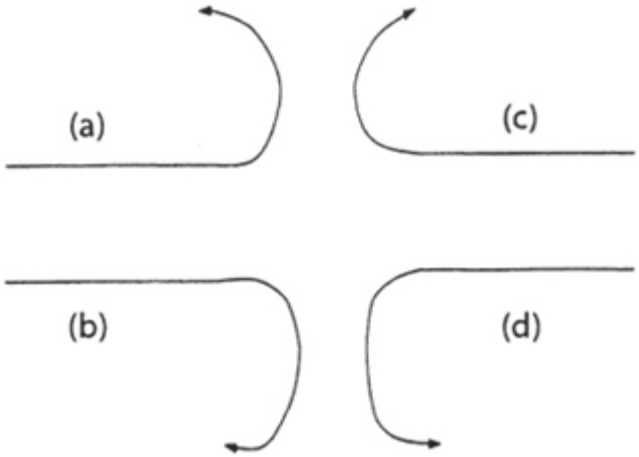


Figure 4.18: Four Possible turning options of fringes.

Previous Next

To locate the point of minimum intensity, eight directions of movement (1-8) are defined (fig.4.19).

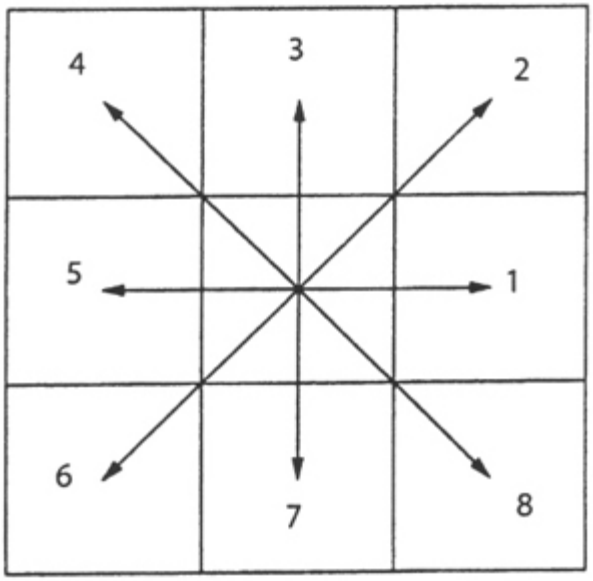


Figure 4.19: Eight possible directions for movements.

The direction in which the minima should be searched is located by placing a template whose size is user-specified at the concerned pixel. While the directions of movement are defined on a $3 \times 3$ template, the intensity minima are computer independently. The choice of size of the template for minimum intensity calculation is related to the fringe thickness. The near wall fringes in the present study were very thin owing to large heat flux. Hence, the choice of the template size was limited to the minimum possible, namely a $3 \times 3$ square. Use of a bigger template is likely to interfere with neighboring fringes and is, hence, undesirable. However, a large template can be used when the fringe bands spread over several pixels. Use of a template as big as $7 \times 7$ and $9 \times 9$ results in an average direction of minimum intensity and tends to produce a smooth tracing. On the other hand, local unphysical variations can be bypassed by using a large template. Hence a $5 \times 5$ template appears to be an optimal choice for interferometric fringes.

more..

Previous Next

### Curve Fitting Approach

In this method, the intensity minima are assumed to coincide with the center of the fringe bands. Specifically, the variations in the grey levels are not made use of. This is equivalent to the classical microscope route of fringe analysis. A few points within each band are collected using a pixel viewing utility available on workstations. The number of points to be collected over an entire fringe depends on the nature of the function to be fitted through the fringe curve. A greater number of points is chosen in the region of sharp changes in the fringe slope. Relatively fewer points are chosen when the fringe shape varies uniformly or is a constant. In the present work, a cubic spline has been fitted through sets of four points while maintaining slope continuity between adjacent data sets. While this methods has the disadvantages of not identifying the minimum intensity location, it does offer certain advantages. These are, thinning of all fringes with no loss and smoothness of the fringe skeleton.

Figure 4.22 shows the thinned images obtained using the curve fitting approach corresponding to the interferograms in Figure 4.20. In the Interferograms for the 90 degree projection, an extra fringe can be seen to be captured. This could not be resolved using the automatic fringe thinning approach. Figure 4.23 shows the thinned images superimposed with the original interferograms. The match is again seen to be good.

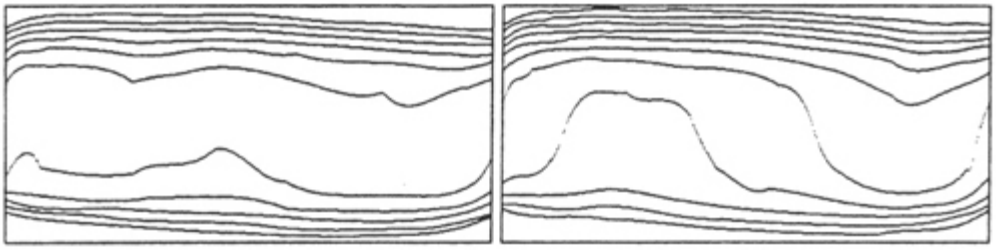

Figure 4.22: Thinned images, 0˚(left) 90˚ (right). curve fitting method for fringe thinning

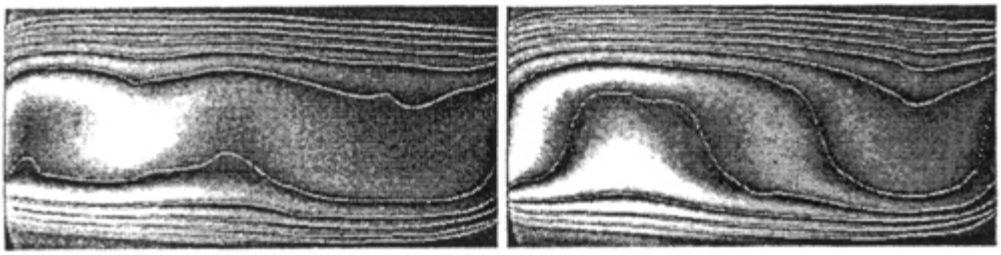

Figure 4.23: Superimposed thinned images (curve fitting method) with original images, 0˚(left) 90˚ (right).

### Paintbrush Drawing

This is a freehand drawing technique where the midpoints within a dark band of the interferogram are approximately located and joined the by a smooth curve. It relies exclusively on eye judgment. The paintbrush utility of the window-95 operating system has been employed in this study. The image containing the fringe curves and the original image are subtracted to get the fringe skeleton. Figure 4.24. shows the thinned images corresponding to the interferograms shown in Figure 4.20. Owing to the manual user-interactive approach, the 90 degree projection has an extra fringe over the image generated by the automatic thinning method (Figure 4.20). The superposition of the original interferograms and the fringe skeleton is shown in Figure 4.25. The paintbrush approach has the disadvantage of not locating the minimum intensity location, but does not require code development and hence is reasonably fast.

Previous Next

## Comparison of Fringe Thinning Algorithms

An implementation of the three thinning algorithms to interferometric fringes reveals the following. The automatic thinning approach is unambiguous and repeatable, in the sense that the thinned fringes do not depend on the starting point specified by the user. The curve fitting and paintbrush approaches are sensitive to the user input. On the other hand, they do not require elaborate code preparation time and can be adopted if thinning is only sporadically required.

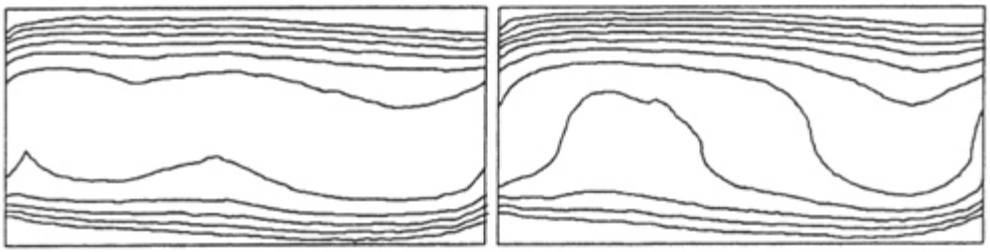

Figure 4.24: Thinned images, 0˚(left) 90˚ (right). paintbrush drawing method for fringe thinning.

A preliminary examination of the thinned images (Fig.4.20,4.22, and 4.25) shown that the three methods produce qualitatively similar results. An independent assessment of these techniques is taken up in the present section. The first criterion adopted is the comparison of the width-averaged temperature profile for each projection. Under nominally steady conditions, i.e., after sufficient time is allowed to elapse, the width-averaged temperature profile in the fluid plotted as a function of the vertical coordinate can be shown to be independent of the projection angle. This is because the total energy transferred across any horizontal plane in the fluid layers is a constant. These profiles are shown in figure 4.26, for all the three algorithms studied. The S-shaped curve, characteristic of buoyancy–driven convection can be seen in this figure. Within experimental limits, a close match between the zero and 90 degree profiles is seen to be realized when the first fringing thinning approach is employed. This match confirms the accuracy of fringe thinning, temperature allocationto fringes, and the absence of interpolation errorss while transferring the data to a rectangular grid. Figure 4.26 also shown that the fringe lost during thinning near the top wall does not degrade energy balance. The agreement in case of the curve-fitting method is partial, while it is unsatisfactory with the paintbrush method.

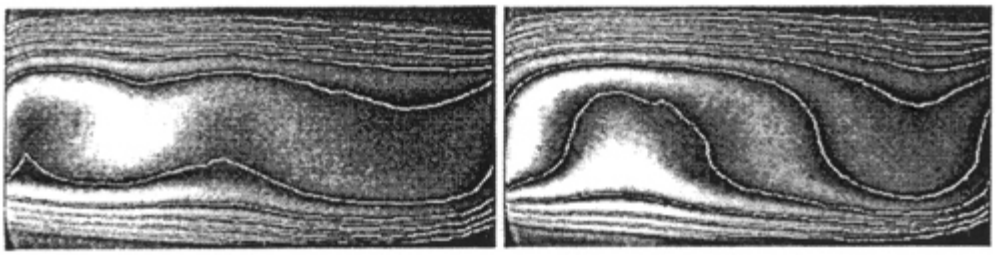

Figure 4.25: Superimposed thinned images (paintbrush method) with original, images 0˚(left) 90˚ (right).

Previous Next

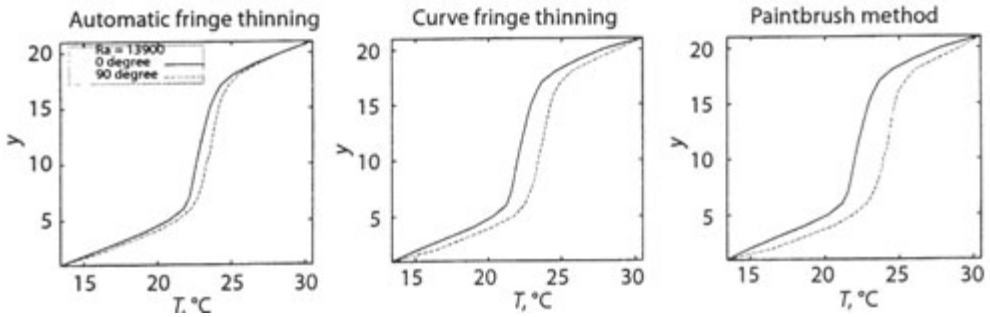


Figure 4.26: Width-averaged temperature profile of the projection temperature field inside a roll.

The tomographic reconstruction of the temperature field using two projections is considered next. The three fringe thinning algorithms are quantitatively evaluated. The three-dimensional temperature field in the fluid layer has been reconstructed using the MART algorithm. The MART algorithm converged asymptotically to a solution for all the three thinning algorithms. Since a correction corresponding to the average of all the rays passing through a pixel was used, a relaxation parameter of unity was used for reconstruction. A convergence criterion of 0.01% between successive updates was employed for stopping the iterations. For each horizontal plane, the number of iterations required was in the range of 30 to 50.

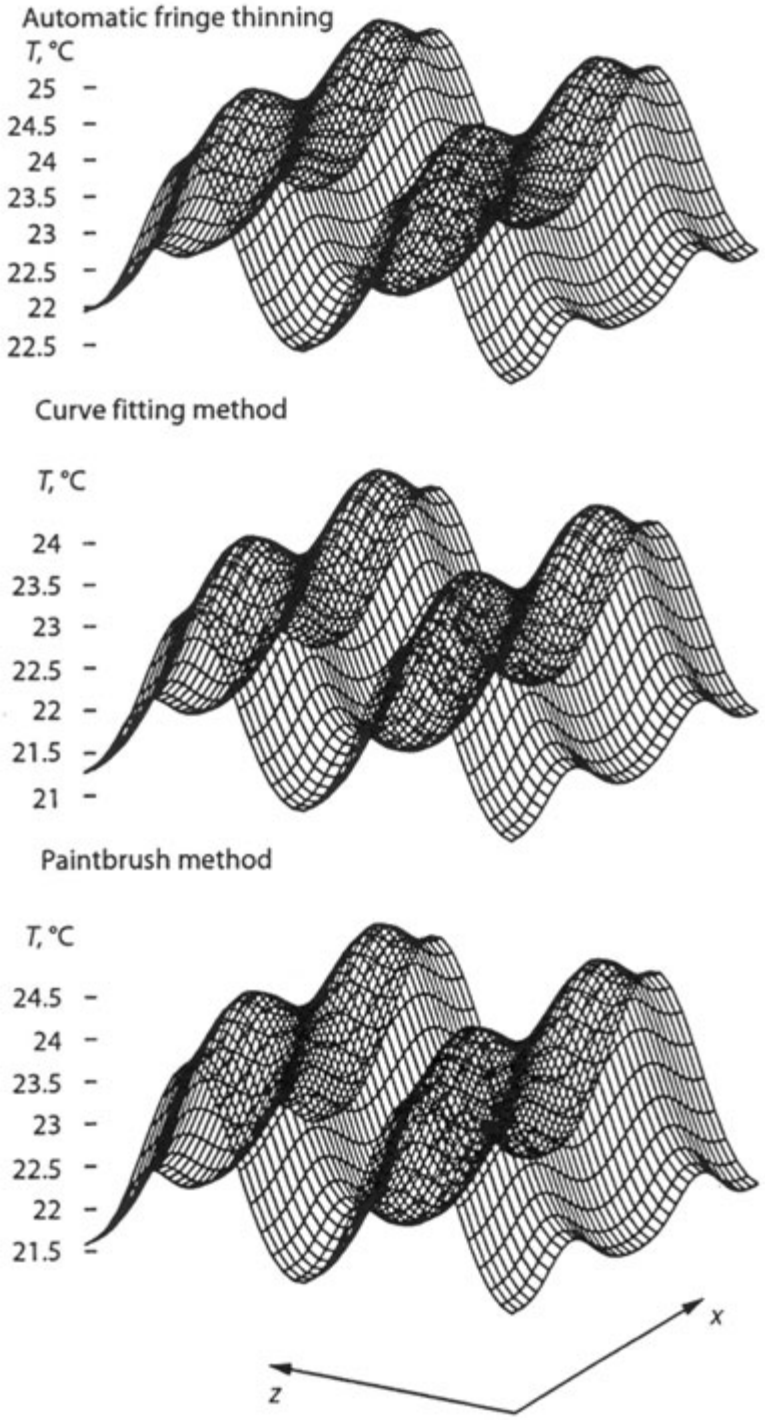


Figure 4.27: Reconstructed temperature surface within the cavity at the central horizontal plane.

more...

Previous Next

## Closure

Three fringe thinning algorithms based on a search for minimum intensity, curve fitting and the paintbrush option available on PCs have been compared in the context of tomographic inversion. The main conclusions that have been drawn from the present study are:

1. The three methods of fringe thinning produce qualitatively similar temperature fields.
2. Quantitative analysis shows differences in the results, but large errors are localized and over 95% of the fluid region, errors are smaller the 1%.
3. The loss of a wall fringe during the automatic fringe thinning does not increase errors either in the reconstructed temperature field or the Nusselt number.
4. The automatic fringe thinning algorithm requires the most code preparation time. It is however superior to the other two methods since it is repeatable and takes the minimum computer time for execution. It is also physical meaningful since it closely satisfies the energy balance criterion.

Previous Next

In experiments, the original as well as partially processed image have superimposed noise. Hence the distribution of intensity across fringes will be ambiguous. Specifically ,the minimum intensity will not strategy be a zero and 8-bit digitization, the maximum will not be 225. Hence the strategy that is preferred is to trace the minima within dark bands and maxima within bright bands, rather than search for points of known intensity. This is the closest approximation that can be achieved in tracking a series of pixels having low-or high-intensities. When a laser is used, one must also take into account the overall Gaussian profile of the light output. Hence, determination of extrema in intensity becomes a local operation in the image domain. Subsequently, the locus of minima or need to be connected within a fringe band across the image, to get a curve on which temperature itself or a temperature-dependent function is a constant.

It is clear that under experimental condition, only intensity minima can be traced since intensity itself is not precisely defined. In practice, one observes a greater noise level in the high-intensity regions, possibly owing to device saturation in the recording medium. This makes locating intensity maxima a difficult task. Hence, fringe thinning operations referred in the present work are related solely to the location of intensity minima in the dark fringe bands.

Several fringe thinning methods are available in the literature. Most of the fringe tracing algorithms that have been suggested are problem–specific and cannot be accepted as generally valid. A large number of published algorithms are based on edge detection by global thresholding, but these are specific to a class of problems and appear to be inapplicable for interferometric images. In the presence of an non-uniform average level of illumination with superimposed noise, the opinion of the present author is that the task of automatic extraction of the fringe skeleton is difficult. This has been experienced even with the well-behaved fringe tracing algorithms given by Robinson [83] and Krishnaswamy [84] for interferometric fringes and by Ramesh and Singh [85] for photoelastic fringe patterns. Funnell [86] has sugessted an easy to implement, but not a fully automatic, technique to trace the fringes. His method is likely to yield good results for low-quality images. In the present study, an algorithm that is similar in approach has been proposed. This algorithm that is similar in approach has been proposed. This algorithmis automatic in the sense that no user input is required at any intermediate stage of the calculation. It is based on the actual two-dimensional grey-level variations and the fringe skeleton is traced by searching alng the minimum intensity direction while simultaneously maintaining connectivity of the point traced.

In the present section, the performance of the fringe thinning algorithms has been evaluated in the context of interferometric image. These images were generated by a Mach-Zehnder interferometer. The experiment performed was one involving Rayleigh-Benard convection. The experiment comprised of a layer of air confined between two horizontal surfaces. The lower surface was heated while the upper surface was cooled, both being maintained respectively at constant temperatures. The vertical side walls that defined the boundaries of the fluid layer were thermally insulated. The temperature differential across the fluid layer led to buoyancy-driven motion, whose pattern could be captured from the fringe patterns. This experiment is described in detail in section 7.3.

The interferograms represent the projection of the three-dimensional temperature field on to a plane. However, the data contained in them must be transferred to a uniform grid before tomographic algorithms can be applied. Several intermediate steps involving image processing operations have to be performed to reach this stage. To start with, interferograms recorded using the CCD camera contain superimposed noise, speckle being the most significant. While speckle is associated with the optical components of the interferometer, the images also carry thermal noise due to edge effects in

the fluid layer. Speckle, as well as thermal noise can be conveniently removed in the Fourier domain by a band–pass filter. An example of the original intensity distribution and that obtained after Fourier-filtering is shown in figure 4.16. The filter is two-dimensional and can remove the high-wave number components of the spectra of the light intensity. The resulting image has blurred edges and must be processed further. The image quality of the filtered image has been enhanced by using utilities such as histogram equalization and high-boost image preparation.

Previous Next

The present discussion is focussed towards fringe thinning and the associated errors. The thinning operations have been carried out with the filtered and enhanced interferograms. Three different approaches have been adopted in this regard: (a) search of the minimum intensity points within the dark band, (b) curve fitting through the centers of the dark band, and (c) freehand tracing of the fringe skeleton using a paintbrush option available in windows-95. These three methods are discussed below in detail.

The temperature corresponding to the individual fringes have been computed using the two known wall temperature and the temperature difference between two successive fringes. Refraction errors have been estimated to be quite small in present experiments. The information available about temperature at fringe locations has been transferred to a two-dimensional grid by using two-dimensional quardratic interpolation. Interpolation errorss have been found to be less than 0.1%. The major source of error betweenthe original interferograms and the data on the interpolated grid was found to be due to fringe thinning alone, other errors owing to filtering for example, being negligible.

The temperature available at this stage for each grid point is a line integral of the temperature field and constitutes the input to the tomographic algorithm. Since refraction errors are small in the present set of experiments, projection data on different horizontal planes can be taken to be independent. Hence, a sequential plane-by-plane reconstruction has been carried out to cover the three dimensions of the cavity. The present discussion on the influence of fringe thinning on tomographic reconstruction is based on two projection angles. Since the number of projections is limited, the algebraic reconstruction technique as against the transform methods has been employed. The use of two orthogonal projection angles is not a limitation because these can still be used to determine the overall features of the dependent variable [88]. Subbarao et al. [32] have evaluated the performance of the algebric reconstruction techniques for interferometric projection data of the temperature field. They have concluded that the multiplicative algebraic reconstruction technique (MART) is best suited in terms of errors and computer time. Hence, in the present work the multiplicative reconstruction technique has been used.

Previous

The direction in which the fringe is to be traced is determined as follows. The sum of the intensities in each of the eight directions are computed and the two sequences of numbers along which the minima occur are searched. The directions producing the minimum intensity sums are accepted as the directions within a fringe band. One of these is the previous direction already identified. Hence the new direction is the one along which the fringe curve has to be extended. In practice the two intensity sums may not be identical since the average intensity level of the image is not constant. Any given pixel will be connected to two neighboring pixels in a thinned image. Hence the past direction of moment has to be preserved to decide the future connections points. Because of residual noise present in the image, it is likely that a pixel may show two new directions in the addition to its last moment. In such a case the sum of intensities that is closer to the previous directions is ignored and the other direction is accepted for the next movement.

The above algorithm can produce loops if precautions are not taken. If a fringe is in the forward tracing mode and the special turning case is not supplied, the fringe is forced to move in the specified direction of (1,2,3,7 and 8) and not (4,5 and 6) the backward direction (fig.4.19). Similarly in backward tracing, the direction (1,2 and 8) is not allowed. If one of the direction that is not permissible during forward tracing is encountered as the final direction of movement, a loop-like structure is formed. Tracing may not be completed in some cases. In Funnell's algorithm [86], user intervention is suggested to circumvent the difficulty. In the present work, the ambiguity is resolved by an iterative procedure as described below.

To avoid the formation of loops the nearest forward direction is found iteractively as follows. Once a reverse direction of movement is encountered, the nearest possible direction is adopted in its place. For example, if the direction of movement is 4 while the tracing is in forward direction, the direction nearest to 4 is 3. Similarly 7 can be replaced by 6. If the direction found is 5, then both 3 and 7 are equally likely. In such a case, the unbiased estimate to 5 is direction 1.

Reallottment of a direction as described above may result in a wrong movement. For example, the direction of movement identified may be one of the previously detected points on the thinned image. In such a case the above steps are repeated and the next closests direction is searched. If the new pixel located falls in one of the four special cases for turning, the image is rotated by 90 degrees in the clockwise direction. Then depending on one of the four cases, one may have to move temporarily in forward of backward directions. During implementation, the code is prepared in a modular fashion to trace forward (to the right) and backward fringes. Rotation of the image enables one of the modules to be used without any change in the market areas of the fringes.

Previous Next

The boundaries of the image, i.e. the window size are to prescribed as an input to the computer code. On reaching the boundary, control in the computer code is transferred to the starting points so that the rest of the fringe in the opposite direction can be traced. The algorithm used for fringe tracing is summarized below:

1. Initialize the thinned image as black (intensity 0).
2. Read the image containing the interferogram including the boundary.
3. Read the starting point data for all the fringes in the image. These points can lie the interior of the image.
4. Specify the desired template size at the starting point.
5. Specify the initial direction of movement to the left or right.
6. Obtain the intensity sums in the eight directions and find the two minima.
7. Start tracing in the direction of the minimum intensity.
8. At the boundary, transfer control to starting point.
9. Start tracing in the opposite direction until the boundary is reached.
10. Assign a grey level of 225 to the traced pixels.
11. Repeat the process for all the fringes.

Figure 4.20 shows the thinned image developed using the procedure given above. Both zero and 90 degree projections are shown.

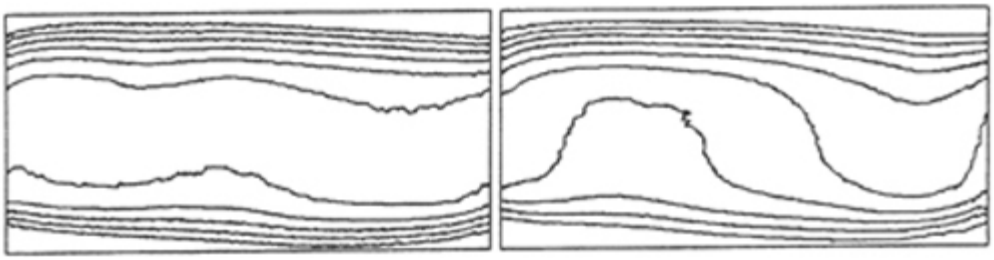

Figure 4.20: Thinned images, $0^{\circ}$ (left) $90^{\circ}$ (right).,automatic fringe thining

Figure 4.21 shows the superposition of the fringe skeleton and the interferograms and the agreement can be seen to be satisfactory. The fringe immediately adjacent to the top wall $(90^{\circ})$ could not be resolved in the sense that a minimum intensity direction could not be identified in certain parts of the image. This could have been taken care of by manually joining the two segments of the fringe. Instead, the unresolved fringe has been deliberately taken to be lost. As discussed later, this was not seen to introduce error in the tomographically reconstructed temperature field. A closer evaluation of the thinning process is taken up in section 4.2

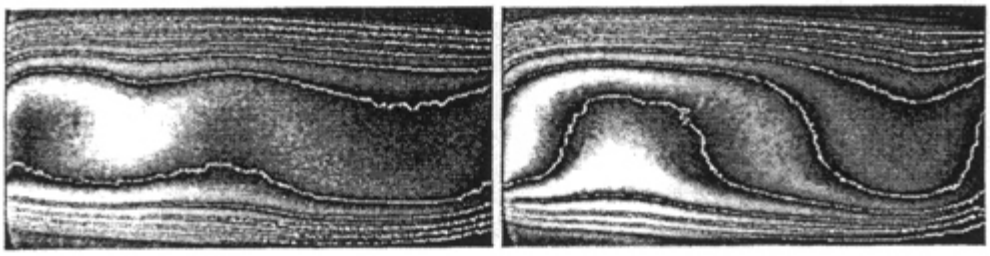

Figure 4.21: Superimposed thinned images (automatic fringe thinning) with

original images, 0˚(left) 90˚ (right).

Previous

Figure 4.27 shows the reconstructed temperature surface along the central plane for all the three thinning algorithms. These surface show the formation of rolls. The rolls show only a minor variation in the $x$ direction and accordingly, may be classifiled as longitudinal, with the roll axis being parallel to the $x$ coordinate. Qualitatively all the three methods display similar results for the temperature field. The formation of longitudinal rolls can be seen with greater clarity with isotherms. The isotherm plots along the midplane of the fluid layer from the automatic thinning algorithm is shown in Figure 4.28. The stretching of isotherms in one direction clearly brings out the orientation of the rolls.

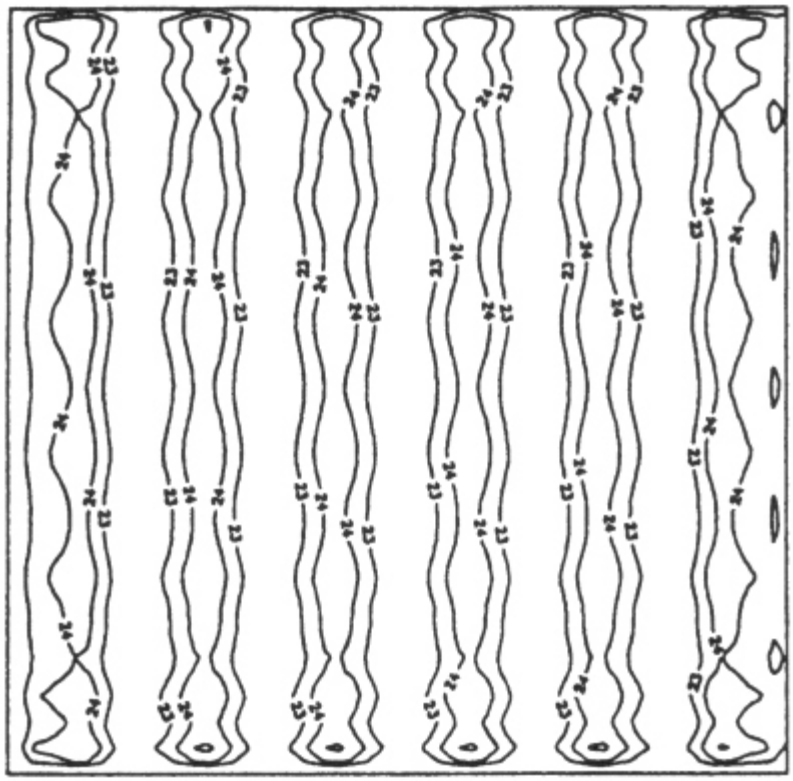

Figure 4.28: Isotherms on the midplane of the fluid layer

Previous Next

A quantitative assessment of the reconstructed temperature field is taken up next. To compute errors, a reference solution is required. Since this is not available for experimental data, the following strategy has been adopted. The temperature field obtained by merging the S-shaped curves in the two projections has been taken as the reference solution. The temperature field thus developed satisfies exactly the energy balance criterion. Errors have been determined between the temperature field developed frsom the thinning algorithms and the reference solution. Errors reported are the absolute maximum error $(\mathrm{E_1 in\,^\circ C})$, the RMS error $(\mathrm{E_2 in\,^\circ C})$ and the percentage RMS error $(E_3)$. The percentage RMS error has been calculated with respect to the temperature different across the fluid layer. The completed fluid layer has been considered while obtaining these quantities. The errors for each thinning algorithm have been summarized in Table 2.

An examination of Table 2 shows that errors associated with the automatic thinning algorithm are uniformly small. The absolute maximum errors with the other algorithms are larger, being in excess of $1^\circ C$. This may not be acceptable in many applications. A comparison of the absolute maximum and RMS errors shows the latter to be smaller, by more than a factor of two. This suggests that large errors are localized over the flow field. The percentage RMS error is truly small for the automatic thinning algorithm, while it is in the range $2-3.5\%$ for the curve fitting and paintbrush methods. This range may still be acceptable in engineering measurement.

Table 2: Reconstruction Errors from the Fringe Thinning Algorithms

| Errors | Automatic Fringe Thinning | Curve Fitting Method | Paintbrush Method |
|---|---|---|---|
| $E_1, ^\circ C$ | 0.034 | 1.51 | 1.03 |
| $E_2, ^\circ C$ | 0.011 | 0.60 | 0.34 |
| $E_3, \%$ | 0.066 | 3.51 | 2.01 |

Previous Next

`

A comparison of the wall heat transfer rates determined from the temperature field is presented next. The dimensionless form of the heat flux, namely the Nusselt number has been determined on the present study. For reasons discussed below, heat fluxes have been computed over one as well as two roll widths at the wall. The wall heat flux is simply the gradient of the field temperature in the near–wall region. It is possible to define a Nusselt number for each hot and cold walls. The average Nusselt number can be computed from the slope of the S-shaped curve shown in Figure 4.26. For comparison, the benchmark result for Nusselt number has been taken from Gebhart et al.[89] This reference value is on a wide variety of experiments reported in the literature and has an uncertainty level of $20\%$.

Figure 4.29 shows the local Nusselt number variation with the $z$ −coordinate over one roll for the three thinning algorithms. Both the hot and cold walls have been considered. The view angle is 90 degrees and so the roll formation is visible in this projection. The roll being inclined, the Nusselt number variation on the two walls are of opposite orientation. The three thinning algorithms qualitatively reproduce these trends. The Nusselt number profile predicted by the automatic thinning algorithm can be seen to be the smoothest of the three. Differences among the three algorithms can be seen to have increased in Figure 4.26, compared to the errors reported in Table 2. This is because the Nusselt number calculated form the three algorithms are within $\pm 10\%$ of one another.

Table 3: Fractional Distribution of $E_1$Error over a Horizontal Plane

| Number of points (%) having error in the range | Automatic fringe thinning | Curve fitting method | Paintbrush method |
|---|---|---|---|
| $> 95\%$ | 0.19 | 0.43 | 0.24 |
| $75 - 95\%$ | 2.09 | 0.24 | 2.0 |
| $50 - 75\%$ | 13.4 | 7.24 | 7.47 |

Previous Next

Figure 4.29 shows the local Nusselt number variation with the $z$ – coordinate over one roll for the three thinning algorithms. Both the hot and cold walls have been considered. The view angle is 90 degrees and so the roll formation is visible in this projection. The roll angle is 90 degrees and so the roll formation is visible in this projection. The roll being inclined, the Nusselt number variation on the two walls are of opposite orientation. The three thinning algorithms qualitatively reproduce these trends. The Nusselt number profile predicted by the automatic thinning algorithm can be seen to be the smoothest of the three. Differences among the three algorithms can be seen to have increased in Figure 4.29, compared to the errors reported in Table 2. This is because the Nusselt number calculated form the three algorithms are within $\pm 10\%$ of one another.

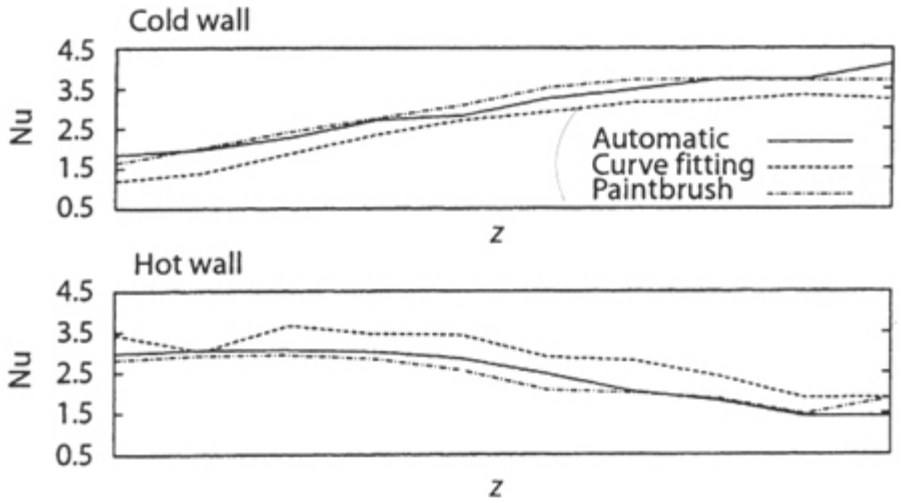


Figure 4.29: Local Nusselt number variation over the hot and cold paltes; comparision of the three thinning algorithms

Table 4 presents the Nusselt number averaged over a single roll in the fluid layer. The automatic fringe thinning algorithm gives Nusselt number that are comparatively close on the two walls. For the zero degrees projection, the average Nusselt number over the two plates differs for both the curve–fitting and the paintbrush methods. The roll in the present study is seen to be formed parallel to the zero degrees axis. These is a considerable mismatch in the average Nusselt number over a single roll as viewed along the $90°$projection data. The cavity-averaged Nusselt number however, is close to the predictions of Gebhart et al. [89]

Table 4: Comparison of Average Nuselt Number Based on the width-averaged temperature

| | Automatic fringe thinning | Curve fitting method | Paintbrush Method | Gebhart et al. |
|---|---|---|---|---|
| 0°, cold | 2.37 | 2.01 | 1.81 | - |
| 0°, hot | 2.38 | 3.14 | 3.11 | - |
| 90°, cold | 2.99 | 2.53 | 3.02 | - |
| | | | | |

| | | | | |
|---|---|---|---|---|
| 90°, hot | 2.41 | 2.88 | 2.34 | - |
| Cavity Average | 2.53 | 2.64 | 2.57 | 2.59 |

Previous Next

To stretch the automatic thinning algorithm to problem of much greater difficulty, the following strategy was adopted. Instead of two, six independent view angles were considered. For each projection, the entire width of the cavity (namely 500mm) was scanned. The average Nusselt number obtained for each projection and for each wall is presented in Table 5. The total average Nusselt number seen here is lower than that predicated by the one-roll data. It is however within the experimental uncertainty of the reference value. As a second check on data reduction, experiments were conducted at a Rayleigh number of 40200. The Nusselt number calculated for the entire fluid layer using the automatic thinning algorithm was found to be 3.32. This value is within 3% of the correlation given by Gebhart et al. [89]

Table5: Average Nusselt Number over the Full Width of the Cavity

| Projection Angle in Degree | Nu (Cold) | Nu (Hot) | Nu (Average) From all angles |
|---|---|---|---|
| 0 | 2.18 | 1.94 | |
| 30 | 2.33 | 2.02 | |
| 60 | 1.99 | 2.34 | |
| 90 | 2.00 | 2.17 | |
| 120 | 2.19 | 2.32 | |
| 150 | 2.27 | 1.95 | |
| | | | 2.14 |

Previous